Production of Chitosan/Zinc Oxide Complex by Ultrasonic Treatment with Antibacterial Activity

Marina SR Barreto[1,2], Cristina T Andrade[1], Edwin G Azero[3], Vânia MF Paschoalin[2] and Eduardo M Del Aguila[2*]

[1]Instituto de Macromoléculas Professora Eloisa Mano, Universidade Federal do Rio de Janeiro, Centro de Tecnologia, Bloco J, Avenida Horácio Macedo 2030, 21941-598 Rio de Janeiro, RJ, Brazil

[2]Instituto de Química, Universidade Federal do Rio de Janeiro, Centro de Tecnologia, Bloco A, Avenida Athos da Silveira Ramos 149, 21941-909 Rio de Janeiro, Brazil

[3]Departamento de Ciências Naturais, Universidade Federal do Estado do Rio de Janeiro, Avenida Pasteur 458, 22290-240 Rio de Janeiro, Brazil

*Corresponding author: Eduardo M Del Aguila, Instituto de Química, Universidade Federal do Rio de Janeiro, Centro de Tecnologia, Bloco A, Avenida Athos da Silveira Ramos 149, 21941-909 Rio de Janeiro, Brazil, Tel: +55 21 39387362; E-mail: emda@iq.ufrj.br

Abstract

This study was conducted with the objective of investigating the physical and antimicrobial properties of structured zinc oxide compounds in chitosan submitted to different times of ultrasonic treatment. Zinc oxide particles were dispersed in water and coated with medium molar mass chitosan and two other sonicated samples, following a simple methodology. Before drying, the chitosan/zinc oxide water suspensions were characterized by rheological tests. Their rheological behavior depended on the period of time during which the chitosan sample was submitted to ultrasound. After drying, the microparticles were characterized by infrared spectroscopy, atomic absorption spectrophotometry and scanning electron microscopy (SEM). The microparticles were investigated as for their particle size distribution (PSD). SEM and PSD results revealed that the chitosan/zinc oxide microparticles had a multimodal dispersion. The antibacterial activity of the neat zinc oxide nanoparticles and of the microparticles was evaluated against *Escherichia coli* and *Staphylococcus aureus*. The results showed that the ZnO nanoparticles had a lower minimum bactericidal concentration (500 µm/mL against *E. coli* and 650 µm/mL against *S. aureus*) than the chitosan-coated/ZnO microparticles. The microparticles with the lowest average particle size and the highest homogeneity exhibited the highest antibacterial activity against both bacteria. This result was attributed to the additional antibacterial activity of soluble zinc ions and of the chitosan sample.

Keywords: Zinc oxide; Chitosan; Antibacterial activity; Ultrasonic treatment

Introduction

Zinc oxide (ZnO) is an effective antibacterial agent because of its high antimicrobial activity, thermal stability and good biocompatibility [1,2]. ZnO reveals high antibacterial activity in a broad spectrum of bacteria, like a *Staphylococcus aureus* and *Escherichia coli* [3,4]. ZnO nanoparticles shows significant bactericidal properties over a broad range of Gram-positive as well as Gram-negative bacteria, such as *Eschericchia coli*, *Staphylococcus enteritidis*, *Bacillus subtillis*, *Staphylococcus aureus*, *Aeromonas aerogene*, *Klebsiella pneumonia*, *Pseudomonas aeruginosa* and *Salmonella typhimurium* [5-10]. Some authors observed that, for both types of bacteria, the damage of cell membranes, followed by leakage of cell contents and cell death, was the result of the antibacterial activity of the oxide. However, the mechanism of zinc oxide antimicrobial activity is still a matter of debate. Generation of hydrogen peroxide (although a weak oxidizer, can provoke cell injure by the Fenton reaction) on its surface was proposed as the main factor related to its antimicrobial effect [11]. Also, cell damage was also attributed to induction of oxidative stress, caused by the generation of other reactive oxygen species (ROS) on the bacteria surface [12,13]. Moreover, accumulation of the nanoparticles on the bacteria surface, stabilized by electrostatic forces [14] and the intrinsic antimicrobial properties of Zn^{2+} ions released by ZnO in aqueous medium [15] were suggested as the cause of cell death. Common conclusions from all those investigations revealed that zinc oxide particle size and concentration have a strong influence on the amount of eradicated Gram-positive and Gram-negative bacteria. The smaller particles have a better antibacterial activity. On the other hand, because of their small size, zinc oxide nanoparticles usually agglomerate, with the deterioration of the desired properties [12,13,16-18]. To prevent particle aggregation, surfactants and polymers are often used as stabilizers, mainly in aqueous environments.

Chitosan is the partially deacetylated derivative of chitin, composed of β-(1,4)-2-amino-2-deoxy-D-glucose and β-(1,4)-2-acetamido-2-deoxy-D-glucose repeating units. It is a nontoxic, biodegradable and biocompatible linear polysaccharide, with biotechnological, biomedical and pharmaceutical applications [19-22]. Chitosan is also known to inhibit the growth of certain microorganisms, probably by the electrostatic binding between its cationic groups to the anionic groups present on the surface of those microorganisms [19]. The antibacterial activity of chitosan was shown to depend on molar mass, degree of acetylation [23] and pH [24].

Ultrasonic treatment is known as a non-conventional, environmentally friendly, and effective method used to promote chemical modifications of polymers [15,25]. Exposing a polymer solution to high intensity ultrasonic radiation seems to have, as primary effect, the reduction of molar mass. The process was reported as nonrandom, and cleavage would occur preferentially near the middle of the chain, without altering the chemical structure of the repeating unit [26,27]. Although data on the effect of chitosan-capped

zinc oxide were found in the literature [28-31], results from a systematic study for the determination of MBC was not yet reported.

In this work, chitosan was chosen as zinc oxide dispersant. Starting from a commercial sample of zinc oxide, nanoparticles were obtained, and used to prepare chitosan-capped zinc oxide particles. The chitosan/zinc oxide particles were characterized. The minimum bactericidal concentration (MBC) of the uncapped and capped particles was determined for *E. coli* (Gram-negative) and *S. aureus* (Gram-positive) bacteria.

Materials and Methods

Materials

The commercial zinc oxide (ZnO) sample was supplied by Brasóxidos Indústria Química Ltda. (Sertãozinho-Mauá, SP, Brazil). Medium molar mass chitosan (CH), with a degree of N-acetylation of DA=0.23 (determined by ^{1}H NMR), was purchased from Polymar Ciência e Nutrição Ltda. (Fortaleza, CE, Brazil). Acetic acid was purchased from Vetec Química Fina (Rio de Janeiro, RJ, Brazil).

Preparation of chitosan solutions

A chitosan stock solution (20 g/L) was prepared at ambient temperature in 1% (v/v) acetic acid, under stirring for 12 h (Sample CH). Aliquots of 100 mL were submitted to sonication for 10 (Sample CH10) and 20 min (Sample CH20) at 40% wave amplitude in a Sonics & Materials Inc. (Newtown, CT, USA) ultrasonic processor, 750 Watt model, operating at 20 kHz, and equipped with a standard probe 13 mm in diameter. The reaction vessel was immersed in an ice-salt-water bath (~0°C) to maintain the samples at a low temperature (~10°C).

Preparation of CH/ZnO, CH10/ZnO and CH20/ZnO particles

Commercial ZnO with average particle size of 0.22 µm, was dispersed in water (Millipore, model Direct-Q3, São Paulo, SP, Brazil) at 4 g/100 mL composition, at 10.000 rpm with a Ultra-Turrax dispersing equipment, for 40 min. Separately, 20 mL of each chitosan solution were dropped under stirring over the ZnO dispersions, and maintained under the same stirring conditions for an additional period of 20 min. At this stage, aliquots of the CSs/ZnO samples were submitted to rheological tests. Then, the samples were centrifuged at 5.000 rpm in a Hitachi Koki centrifuge, model Himac CR22GII (Tokyo, Japan), extensively washed with purified water, and spray-dried in a Labmaq equipment, model MSD 1.0 (Labmaq do Brasil, Ribeirão Preto, SP, Brazil) at 140°C and 1 L/h rate.

Physicochemical and morphological characterizations

X-ray diffraction (XRD): The XRD curve for the sonicated ZnO sample was obtained with a Miniflex diffractometer (Rigaku Corporation, Osaka, Japan) operating at CuK$_\alpha$ wavelength of 1.542 A. The sample was exposed to the X-ray beam with the X-ray generator running at 30 kV and 15 mA. Scattered radiation was detected at ambient temperature in the angular region (2θ) of 2-80° at a rate of 3°/min and a step size of 0.05°. The diffractogram was smoothed (Savitsky-Golay, polynome=2, points=7), and the baseline was corrected.

Rheological measurements: Rheological measurements were performed at 25°C using a controlled stress rheometer AR G2 (TA Instruments Inc., New Castle, DE, USA) fitted with a cone-and-plate geometry (2° cone angle, 40 mm diameter, 54 µm gap). Strain sweep was measured first as the evolution of the complex modulus at 6.28 rad s^{-1} for the determination of the linear viscoelastic region. Then, frequency sweep (mechanical spectra) was measured from 10^{-1} to 10^2 rad s^{-1} (at strain value of 1%), within the viscoelastic region. Finally, steady state flow was performed from 10^{-1} to 10^2 s^{-1} shear rates, first in increasing order and then in decreasing order of applied torque.

Infrared spectroscopy (FTIR): ZnO, CH/ZnO, CH10/ZnO and CH20/ZnO samples were characterized by FTIR spectroscopy in a Excalibur Series Fourier transform spectrometer, model 3100 (Varian Inc., Palo Alto, CA, USA) as KBr disks.

Atomic absorption spectrophotometry (AAS): The zinc contents were determined according to the standard AOAC method (2005) using a Varian AA280 atomic absorption spectrometer (Les Ulis, France). Each sample was heated at 550°C and the ash boiled with 10 mL of 20% HCl in a beaker and then filtered into a 100 mL standard flask. All samples were analyzed in triplicate.

Scanning electron microscopy (SEM): Samples were visualized with a FEI Quanta^{TM} 400 (Hillsboro, OR, USA) scanning electron microscope, at the acceleration voltage of 20 kV. The samples were vacuum-coated with gold before measurements.

Determination of particle size distribution: Particle size distribution (PSD) of the samples was determined by laser diffraction, using a Malvern equipment, model Masterisizer 2000 (Malvern Instruments, Malvern, UK). The samples were dispersed in water in the Hydro 2000SM apparatus up to the laser obscuration index reached 10-12%. The PSD values for the samples were determined in triplicate and were expressed as equivalent volume diameters at 10% (d_{10}%), 50% (d_{50}%) and 90% (d_{90}%) of the cumulative volume, as the average of the diameter values ($D_{4,3}$) and Span. The Span values indicated the particle polydispersity and they were calculated according to Equation 3.

$$Span = \frac{d90\% - d10\%}{d50\%} \qquad (Equation-3)$$

Biological Activity

Determination of the minimum bactericidal concentration (MBC)

The minimum bactericidal concentration (MBC) of the samples (ZnO, CH/ZnO, CH-10/ZnO eCH-20/ZnO) was tested by well diffusion method and a liquid growth-inhibition assay against *E. coli* DH5α strain and *S. aureus* ATCC 6538 (INCQS-Fiocruz), Gram negative and positive microbes, respectively. The same assay was performed to investigate the antimicrobial activity of the chitosan used in the formulation of the samples. The strains were grown in LB medium (Luria-Bertani BD™) in an orbital shaker at 200 rpm, 37°C, for 24 h. The cellular density was adjusted in saline solution (0.8% of NaCL) to the turbidity equivalent to McFarland 0.5 standard (1.5×10^8 CFU/mL) and it was used as an inoculum in presence of different concentrations of the samples at 37°C for 18 h at 200 rpm. After that, cells were serially diluted in saline solution (0.8% of NaCL), plated on solid LB, and incubated at 37°C for 18 h. The experimental controls were carried out at the same conditions without samples produced.

Colony-forming units were counted. The MBC was taken as the concentration at which 100% of growth inhibition was observed [32].

Results and Discussion
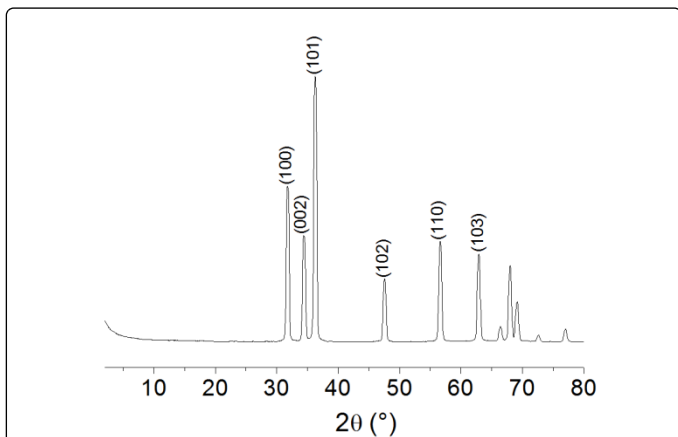
Figure 1: X-ray diffractogram in the 2θ region of 2.0° to 80° for the ZnO dispersed sample.

Sonication has been proposed as a method to obtain well-dispersed ZnO nanoparticles [33,34]. In a recent publication, a double-layered hydroxide was submitted to different dispersing methods, and the use of a Turrax equipment was shown to lead to better results [35]. With the same purpose, a commercial sample of ZnO was dispersed in water at 10.000 rpm. In the XRD diffractogram (Figure 1), obtained for the dispersed sample, the most intense reflections, at 31.75°, 34.40° and 36.3°, were attributed to the (100), (002) and (101) planes. The observed reflections can be indexed to the hexagonal ZnO phase (wurtzite structure). The crystallite size (D_{XRD}=40 nm) was calculated from the Scherrer's formula applied to the most intense reflection.

Because of interparticle attraction, small particles in a liquid have the tendency to aggregate. To prevent aggregation and sedimentation of high-surface energy metal oxides nanometric particles, CH was chosen as the stabilizing polymer. The rheological properties were investigated for the chitosan/ZnO suspensions before centrifugation. The variation of storage (G') and loss (G") moduli values as a function of frequency (mechanical spectra) for the CH/ZnO and CH20/ZnO samples are shown in Figure 2a. As described before, the CH20/ZnO sample was prepared after sonication of CH for 20 min; therefore, the CH20 sample had its molar mass severely reduced. Comparing the curves obtained for the systems, both of them presented a predominantly elastic behavior (G'>G"), characterized by a low rubbery plateau (at low frequencies). Although elastic, the low values indicated the formation of rather fragile structures. The differences between the behaviors of the CH/ZnO and CH20/ZnO systems seems to be related to the biopolymers molar masses and, consequently, to their adsorption to the inorganic nanoparticles.
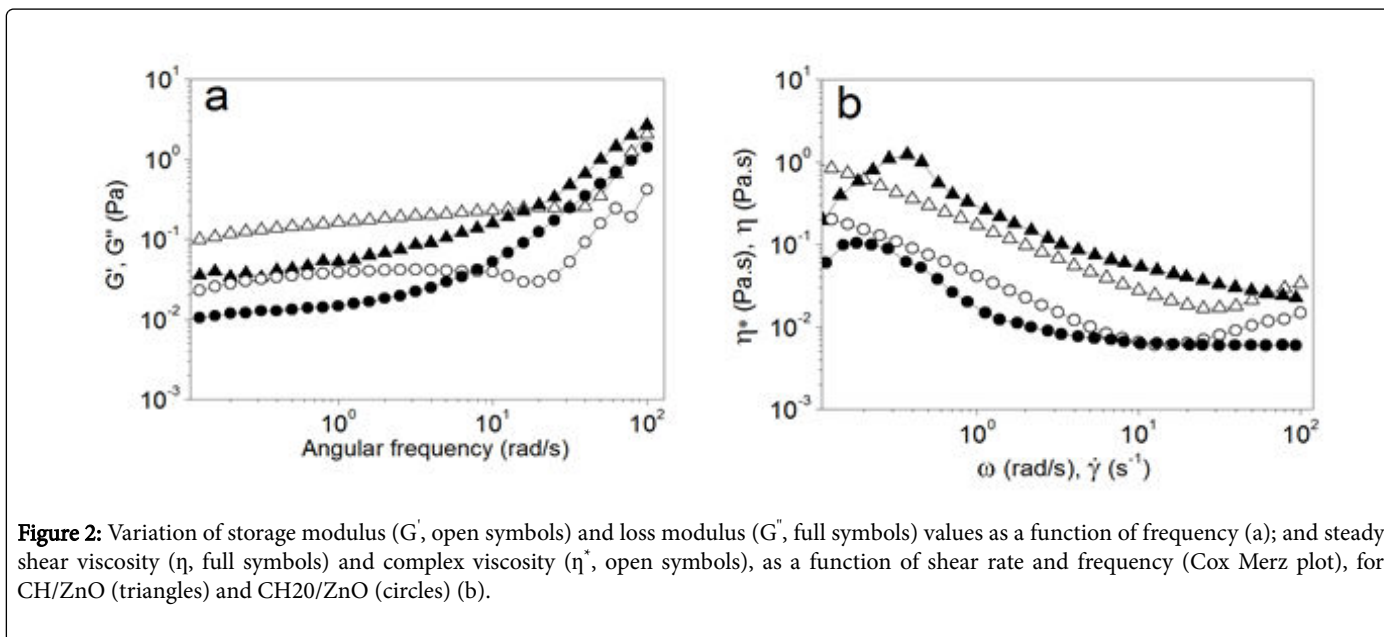
Figure 2: Variation of storage modulus (G', open symbols) and loss modulus (G", full symbols) values as a function of frequency (a); and steady shear viscosity (η, full symbols) and complex viscosity (η*, open symbols), as a function of shear rate and frequency (Cox Merz plot), for CH/ZnO (triangles) and CH20/ZnO (circles) (b).

For a high-molar-mass polymer, such as CH, it would be difficult for all segments of a chain to be adsorbed onto a particle surface. Loops might be formed, and the same chain might be adsorbed onto many nanoparticles, eventually leading to the so-called bridging flocculation [36]. On the other hand, for the lower-molar-mass CH20, the possibility of a chain to be adsorbed to a lower number of nanoparticles, gave rise to a different rheological response, revealing the second G'-G" crossover at a lower frequency value (~8 rad/s).

In Figure 2b, the magnitude of the steady-shear viscosity (η) and the magnitude of the complex viscosity (η*) were compared at equal values of shear rate and oscillatory frequency (Cox Merz plot), for CH/ZnO

and CH20/ZnO samples. As expected, these suspensions do not follow the Cox-Merz correlation. It is worth observing the shear thinning behavior of both samples. Also, shear flow affected the systems differently, depending on the length of the biopolymer chain, being more disturbing for the structure of CH20/ZnO. For this sample, the curve of steady-shear viscosity seems to reveal a Newtonian plateau at low shear rates and two shear thinning regions; the first at intermediate shear rates and the second (smoother) at higher shear rates. Moreover, the complex viscosity curves obtained for CH/ZnO and Zn20/ZnO, following a region of decreasing values, showed a region in which the viscosity was partially recovered. This result

reflected the behavior of the elastic modulus in the transition region, after the observed crossover.

In Figure 3, the FTIR spectrum obtained for the ZnO sample (Figure 3a, trace I) showed a low-intensity band at 3490 cm^{-1}, attributed to O-H stretching vibrations, probably from humidity. The high-intensity band at 490 cm^{-1} was attributed to Zn-O stretching vibration. Other very weak absorptions were attributed to C=O and C-O stretching vibrations of the precursor zinc diacetate [37]. In trace II (Figure 3a), the FTIR spectrum for CH showed a broad band with high intensity, and a maximum at 3440 cm^{-1}, which was attributed to O-H

and N-H stretching vibrations of chitosan. The absorptions at 1650 and 1590 cm^{-1} were attributed to amide I (C=O stretching vibrations) and amide II (C-N stretching and C-N-H bending vibrations) of amides in the solid state. The high-intensity band around 1100 cm^{-1} is characteristic of asymmetrical C-O-C stretching vibration. For the samples CH/ZnO, CH10/ZnO and CH20/ZnO, the FTIR spectra of Figure 3b (traces I, II and III, respectively), showed the absorption already observed for ZnO and CH, similarly reported by other authors [38].
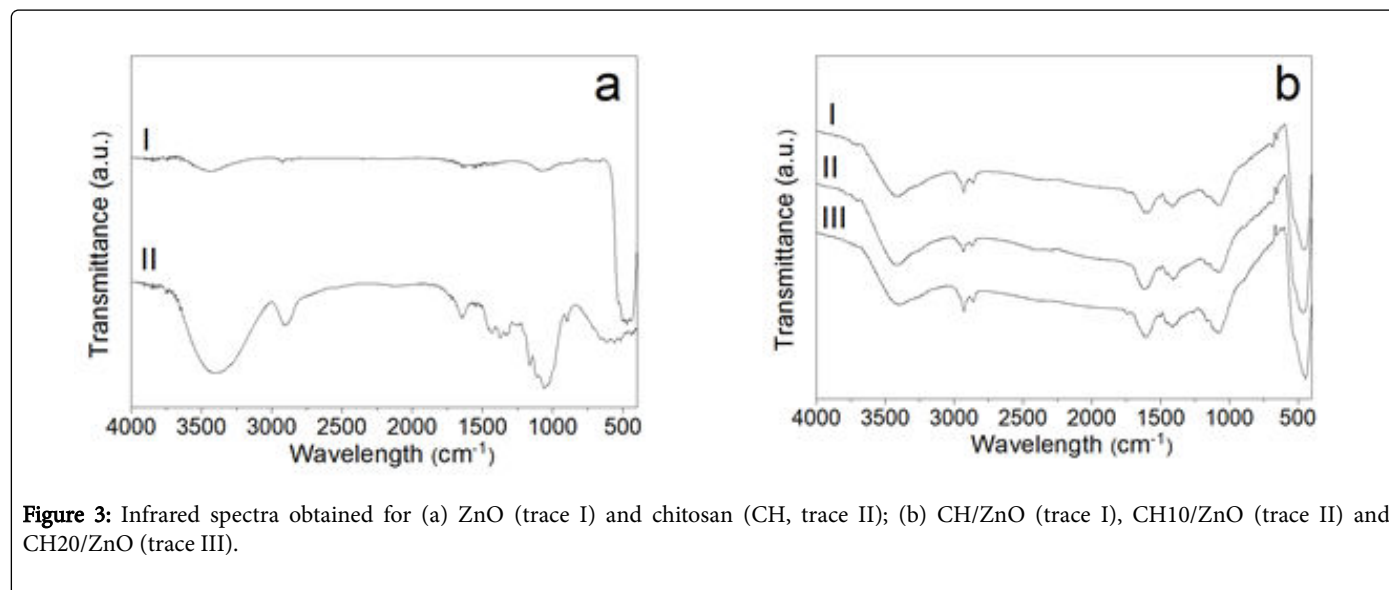
Figure 3: Infrared spectra obtained for (a) ZnO (trace I) and chitosan (CH, trace II); (b) CH/ZnO (trace I), CH10/ZnO (trace II) and CH20/ZnO (trace III).

The morphology and particle size distribution of the chitosan/ZnO microparticles were also characterized. The SEM images, obtained for the three samples (Figure 4), revealed spherical particles with rough surfaces, typical of spray-dried powers. The particles exhibited various sizes, but the majority of those with larger sizes does not seem to be formed from agglomeration. More information was provided by the curves of Figure 5, which show the size distribution for the samples and their volume percentage. Microparticles presented a multimodal distribution with partially-resolved peaks. Size heterogeneity was already suggested by the SEM images and, depending on the time the chitosan solution spent under ultrasound (0, 10 or 20 min), particles with relatively more homogeneous and reduced sizes were obtained. Average sizes of 16.29, 8.03 and 7.94 μm was observed for CH/ZnO, CH10/ZnO and C20/ZnO microparticles by laser diffraction (Table 1). This result, as well as those found for the majority of microparticles ($d_{90\%}$), corroborates the idea previously stated on the differences of polymer/nanoparticle adsorption and encapsulation, according to differences in molar mass [36]. Also, the dispersity in particle size was more pronounced for the CH/ZnO microparticles, and decreased with the increasing time chitosan was submitted to ultrasound.

Sample	$d_{10\%}$ (μm)	$d_{50\%}$ (μm)	$d_{90\%}$ (μm)	$d_{4,3}$ (μm)	Span (μm)
CH/ZnO	0.54	2.23	60.44	16.29	26.91
CH10/ZnO	0.55	3.15	19.73	8.03	6.09

CH20/ZnO	0.48	1.13	4.25	7.94	3.33

Table 1: Diameters of the chitosan/zinc oxide microparticles without sonication of chitosan (CH/ZnO sample), and with chitosan submitted to sonication for 10 min (CH10/ZnO sample) and 20 min (CH20/ZnO sample).

Samples	Sample concentration (μg/mL)	Concentration of retained Zn^{2+} (μg/mL)[1]	E. coli inhibition (%)
ZnO	200	200	12.65 ± 0.71
	500	500	100 ± 0.00
CH/ZnO	200	182	5.82 ± 0.55
	500	455	47.7 ± 1.51
	1000	910	100 ± 0.00
CH10/ZnO	200	190	4.94 ± 1.63
	500	475	35.8 ± 1.18
	1000	950	100 ± 0.00
CH20/ZnO	200	156	5.42 ± 1.05
	500	390	37.14 ± 0.90

	1000	780	100 ± 0.00

Table 2: Antimicrobial activity of the samples against *Escherichia coli*. [1]Average concentration of retained Zn^{2+} as determined by atomic absorption spectrophotometry: ZnO, 100 mass%; CH/ZnO, 91 mass%; CH10/ZnO, 91 mass%; CH20/ZnO, 78 mass%.

The MBC values for the microparticle samples, against model Gram-negative and Gram-positive bacteria, were determined and are shown in Tables 2 and 3, respectively. The ZnO neat sample was effective to *E. coli* and *S. aureus* at the concentrations of 500 and 650 μm/mL, respectively. *S. aureus* was slightly more resistant than *E. coli*. Similar result was observed by other authors [9,39] and attributed to several factors, among them to the intrinsic nature of the cell wall in Gram-negative and Gram-positive bacteria. The cell wall of Gram-negative bacteria, such as *E. coli*, consists of a thin layer of peptidoglycan in the periplasmic space between the inner and outer lipid membranes.
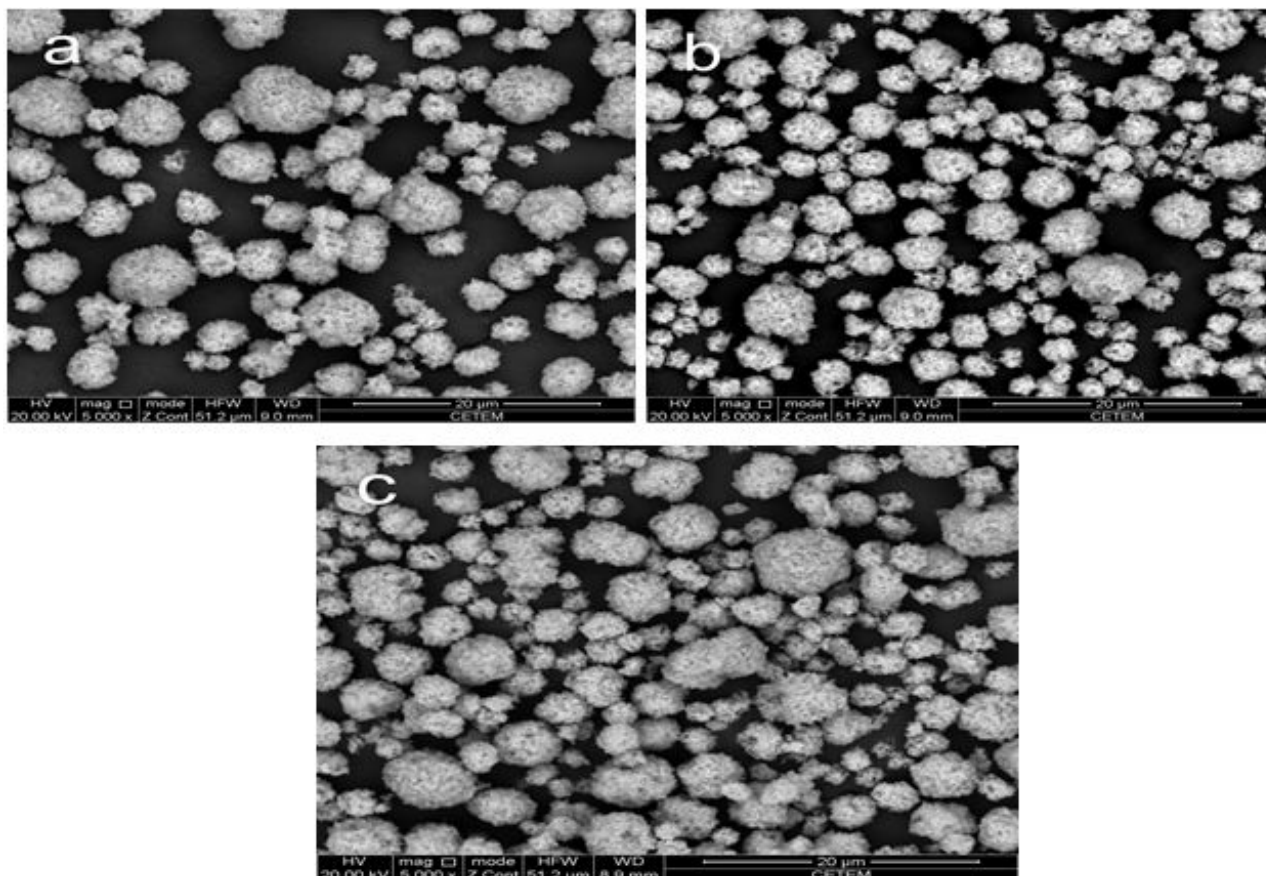
Figure 4: SEM images obtained for CH/ZnO (a), CH10/ZnO (b) and CH20/ZnO (c) microparticles.

On the other hand, the cell wall of *S. aureus* (Gram-positive bacteria) have a single lipid membrane surrounded by a cell wall composed of a thick layer of peptidoglycan and lipoteichoic acid [40]. Moreover, carotenoid pigments and antioxidant enzymes, which are also present in the cell wall, contribute to the resistance of *S. aureus* against oxidizing agents [41].

Tables 2 and 3 also show that the MBC value determined for the neat ZnO nanoparticle is lower than those determined for the chitosan-coated ZnO microparticles. The possibility of chitosan to be acting as a barrier to the migration of ZnO to the medium might be suggested as an explanation. However, a different result was reported previously, for commercial low molar mass chitosan-capped ZnO nanorods [28]. Very probably, the molar mass of the sample used by these authors was much lower than those of CH10 and CH20, the differences in molar mass of the CH components and the methodology used to prepare the particles might explain the contradictory results.

Apparently, the chitosan-coated ZnO microparticles showed the same MBC (1000 μg/mL) against both bacteria. However, the data should be evaluated in relation to the Zn^{2+} concentration retained in the samples [15], as determined by AAS (Tables 2 and 3). In this case, the CH20/ZnO sample (with the lowest average particle size and highest size homogeneity) exhibited the highest antibacterial activity at 1000 μg/mL. Thus, while CH/ZnO and CH10/ZnO at 1000 μg/mL, with respectively 910 μg/mL and 950 μg/mL of retained Zn^{2+}, resulted in *E. coli* and *S. aureus* being inactivated by 100%, to inactivate 100% of bacteria colonies with the CH20/ZnO sample, a concentration of retained Zn^{2+} of only 780 μg/mL was necessary. This result might be explained by (i) CH20 formed a thinner film around ZnO particles, which facilitated its migration toward the exterior of the

microparticles; (ii) CH20, with the lowest molar mass, by itself contributed more significantly to the antimicrobial activity, as reported by several authors [23,24]. In CH20/ZnO microparticles, the soluble zinc ions, with a significant contribution to the antibacterial activity [15], might be assumed to be formed faster in the culture medium. Other mechanisms of antibacterial activity, such as the generation of reactive oxygen and the direct contact of ZnO with bacteria cell surface, would be also favored.

Samples	Sample concentration (µg/mL)	Concentration of retained Zn^{2+} (µg/mL)[1]	S. aureus inhibition (%)
ZnO	200	200	45.6 ± 1.30
	500	500	63.5 ± 1.39
	650	650	100 ± 0.00
CH/ZnO	250	227.5	42.9 ± 1.44
	700	637	59.2 ± 0.72
	1000	910	100 ± 0.00
CH10/ZnO	250	237.5	35.7 ± 1.04
	700	665	54.3 ± 1.08
	1000	950	100 ± 0.00
CH20/ZnO	250	195	35.42 ± 0.39
	700	546	57.25 ± 0.66
	1000	780	100 ± 0.00

Table 3: Antimicrobial activity of the samples against *Staphylococcus aureus*. [1]Average concentration of retained Zn^{2+} as determined by atomic absorption spectrophotometry: ZnO, 100 mass%; CH/ZnO, 91 mass%; CH10/ZnO, 91 mass%; CH20/ZnO, 78 mass%.
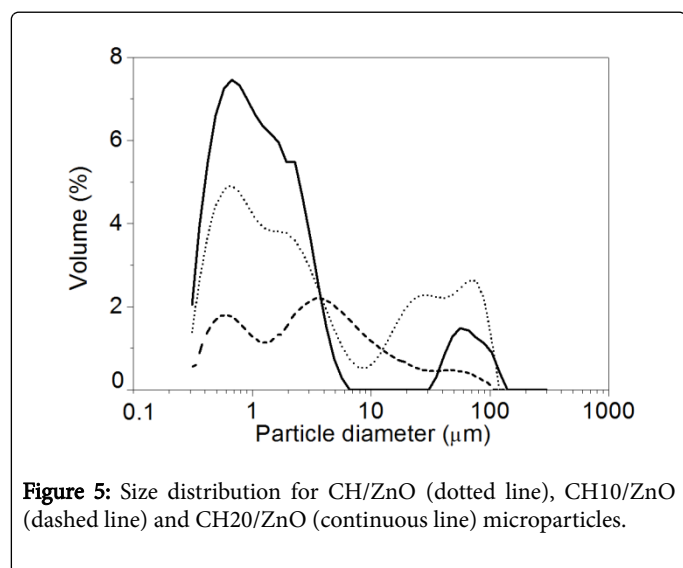
Figure 5: Size distribution for CH/ZnO (dotted line), CH10/ZnO (dashed line) and CH20/ZnO (continuous line) microparticles.

Conclusion

Chitosan/zinc oxide complexes were prepared using chitosan samples and ultrasound radiation. Chitosan/zinc oxide suspensions presented a soft solid-like character, revealed by oscillatory rheological tests, and a shear-thinning behavior under steady-shear flow and for the chitosan/zinc oxide microparticles, differences were detected in relation to average particle size and dispersity. CH sample sonicated for longer periods of time led to ZnO microparticles (CH20/ZnO) with the lowest average particle size and the lowest dispersity and only the ZnO neat particles showed a slightly increased activity against *E. coli* compared to their activity against *S. aureus*. The MBC of the microparticles against both bacteria was better evaluated by considering the average concentration of retained zinc ions and the best antibacterial activity was determined for CH20/ZnO microparticles, in which the low viscosity chitosan would form a thinner film around ZnO particles. This would facilitate ZnO migration toward the exterior of the microparticles and the fast formation of zinc ions in the culture medium. The lower molar mass of CH20, submitted to sonication for longer periods of time, would also contribute to the lowest MBC.

References

1. Ambika S, Sundrarajan M (2015) Antibacterial behaviour of Vitex negundo extract assisted ZnO nanoparticles against pathogenic bacteria. J Photochem Photobiol B 146: 52-57.

2. Svetlichnyi V, Shabalina A, Lapin I, Goncharova D, Nemoykina A (2016) ZnO nanoparticles obtained by pulsed laser ablation and their composite with cotton fabric: Preparation and study of antibacterial activity. App Surf Sci 372: 20-29.

3. Shim K, Abdellatif M, Choi E, Kim D (2017) Nanostructured ZnO films on stainless steel are highly safe and effective for antimicrobial applications. Appl Microbiol Biotechnol 101: 2801-2809.

4. Panigrahi J, Behera D, Mohanty I, Subudhi U, Nayak BB, et al. (2011) Radio frequency plasma enhanced chemical vapor based ZnO thin film deposition on glass substrate: A novel approach towards antibacterial agent. App Surf Sci 258: 304-311.

5. Tam KH, Djurišic AB, Chan CMN, Xi YY, Tse CW, et al. (2008) Antibacterial activity of ZnO nanorods prepared by a hydrothermal method. Thin Solid Film 516: 6167-6174.

6. Azam A, Ahmed AS, Oves M, Khan MS, Habib SS, et al. (2011) Antimicrobial activity of metal oxide nanoparticles against Gram-positive and Gram-negative bacteria: a comparative study. Int J Nanomedicine 7: 6003-6009.

7. Luo Z, Wu Q, Xue J, Ding Y (2013) Selectively enhanced antibacterial effects and ultraviolet activation of antibiotics with ZnO nanorods against Escherichia coli. J Biomed Nanotechnol 9: 69-76.

8. Zhang L, Li Y, Liu X, Zhao L, Ding Y, et al. (2013) The properties of ZnO nanofluids and the role of H2O2 in the disinfection activity against Escherichia coli. Water Res 47: 4013-4021.

9. Jain A, Bhargava R, Poddar P (2013) Probing interaction of Gram-positive and Gram negative bacterial cells with ZnO nanorods. Mater Sci Eng C Mater Biol Appl 33: 1247-1253.

10. Yousef JM, Danial EN (2012) In Vitro antibacterial activity and minimum inhibitory concentration of zinc oxide and nano-particle zinc oxide against pathogenic strains. J of Health Sci 2: 38-42.

11. Ansari MA, Khan HM, Khan AA, Sultan A, Azam A (2012) Synthesis and characterization of the antibacterial potential of ZnO nanoparticles against extended-spectrum ß-lactamases-producing Escherichia coli and

Klebsiella pneumoniae isolated from a tertiary care hospital of North India. Appl Microbiol Biotechnol 94: 467-477.

12. Jiang Y, Zhang L, Wen D, Ding Y (2016) Role of physical and chemical interactions in the antibacterial behavior of ZnO nanoparticles against E. coli. Mater Sci Eng C Mater Biol Appl 69: 1361-1366.

13. Applerot G, Lipovsky A, Dror R, Perkas N, Nitzan Y, et al. (2009) Enhanced antibacterial activity of nanocrystalline ZnO due to increased ROS-mediated cell injury. Adv Funct Mat 19: 842-852.

14. Zhang L, Ding Y, Povey M, York D (2008) ZnO nanofluids – A potential antibacterial agent. Prog in Nat Sci: Mat Inter 18: 939-944.

15. Pasquet J, Chevalier Y, Pelletier J, Couval E, Bouvier D, et al. (2014) The contribution of zinc ions to the antimicrobial activity of zinc oxide. Colloid and Surf A 457: 263-274.

16. Bian SW, Mudunkotuwa IA, Rupasinghe T, Grassian VH (2011) Aggregation and dissolution of 4 nm ZnO nanoparticles in aqueous environments: Influence of pH, ionic strength, size, and adsorption of humic acid. Langmuir 27: 6059–6068.

17. Zhou D, Keller AA (2010) Role of morphology in the aggregation kinetics of ZnO nanoparticles. Water Res 44: 2948-2956.

18. Liu WS, Peng YH, Shiung CE, Shih YH (2012) The effect of cations on the aggregation of commercial ZnO nanoparticle suspension. J of Nanopart Res 14: 1259-1268.

19. Muxika A, Etxabide A, Uranga J, Guerrero P, de la Caba K (2017) Chitosan as a bioactive polymer: Processing, properties and applications. Int J Biol Macromol 17: 31757-31781.

20. Rinaudo M (2006) Chitin and chitosan: Properties and applications, Progress in Poly Sci 31: 603-632.

21. Muzzarelli RA (2010) Chitins and chitosans as immuno adjuvants and non-allergenic drug carriers. Mar Drugs 8: 292-312.

22. Dash M, Chiellini F, Ottenbrite RM, Chiellini E (2011) Chitosan—A versatile semisynthetic polymer in biomedical applications. Prog Poly Sci 36: 981-1014.

23. Pavinatto A, Pavinatto FJ, Delezuk JAM, Nobre TM, Souza AL, et al. (2013). Low molecular-weight chitosans are stronger biomembrane model perturbants. Colloids Surf B Biointerfaces 104: 48-53.

24. Younes I, Sellimi S, Rinaudo M, Jellouli K, Nasri M (2014) Influence of acetylation degree and molecular weight of homogeneous chitosans on antibacterial and antifungal activities. Int J Food Microbiol 185: 57-63.

25. Baxter S, Zivanovic S, Weiss J (2005) Molecular weight and degree of acetylation of high-intensity ultrasonicated chitosan, Food Hydrocolloids 19: 821-830.

26. Price GJ, Smith PF (1993) Ultrasonic degradation of polymer solutions. III. The effect of changing solvent and solution concentration. Euro Polym J 29: 419-424.

27. Sathiskumar PS, Madras G (2012) Ultrasonic degradation of butadiene, styrene and their copolymers. Ultrason Sonochem 19: 503-508.

28. Bhadra P, Mitra MK, Das GC, Dey R, Mukherjee (2011) Interaction of chitosan capped ZnO nanorods with Escherichia coli. Mat Sci Eng C 31: 929-937.

29. Jayasuriya AC, Aryaei A, Jayatissa AH (2013) ZnO nanoparticles induced effects on nanomechanical behavior and cell viability of chitosan films, Mat Sci Eng C 33: 3688-3696.

30. Rahman M, Muraleedaran K, Mujeeb VMA (2015) Applications of chitosan powder with in situ synthesized nano ZnO particles as an antimicrobial agent, Int J of Biol Macromol 77: 266-272.

31. Youssef AM, Abou-Yousef H, El-Sayed SM, Kamel S (2015) Mechanical and antibacterial properties of novel high performance chitosan/ nanocomposite films. Int J Biol Macromol 76: 25-32.

32. Wu M, Hancock RE (1999) Interaction of the cyclic antimicrobial cationic peptide bactenecin with the outer and cytoplasmic membrane. J Biol Chem 274: 29-35.

33. Matsuyama K, Mishima K, Kato T, Irie K, Mishima K (2012) Transparent polymeric hybrid film of ZnO nanoparticle quantum dots and PMMA with high luminescence and tunable emission color. J Colloid Interface Sci 367: 171-177.

34. Khorsand Zak A, Majid WH, Wang HZ, Yousefi R, Moradi Golsheikh A, et al. (2013) Sonochemical synthesis of hierarchical ZnO nanostructures. Ultrason Sonochem 20: 395-400.

35. Carmo DM, Oliveira MG, Soares, Bluma G (2014) Effect of the dispersive method in the preparation of the polyurethane/hydrotalcite nanocomposites by in situ polymerization. App Clay Sci 101: 128-135.

36. Nasu A, Otsubo Y (2006) Rheology and UV protection properties of suspensions of fine titanium dioxides in a silicone oil. J Colloid Interface Sci 296: 558-564.

37. Alias SS, Ismail AB, Mohamad AA (2010) Effect of pH on ZnO nanoparticle properties synthesized by sol-gel centrifugation. J Alloy Comp 499: 231-137.

38. Saeed SES, El-Molla MM, Hassan ML, Bakir E, Abdel-Mottaleb MMS, et al. (2014) Novel chitosan-ZnO based nanocomposites as luminescent tags for cellulosic materials. Carbohydr Polym 89: 817-824.

39. Trandafilovic LV, Bozanic DK, Dimitrijevic-Brankovic S, Luytc AS, Djokovic V (2012) Fabrication and antibacterial properties of ZnO– alginate nanocomposites. Carbohydr Polym 88: 263-269.

40. Brown L, Wolf JM, Prados-Rosales R, Casadevall A (2015) Through the wall: extracellular vesicles in Gram-positive bacteria, mycobacteria and fungi. Nat Rev Microbiol 13: 620-630.

41. Liu GY, Essex A, Buchanan JT, Datta V, Hoffman HM, et al. (2005) Staphylococcus aureus golden pigment impairs neutrophil killing and promotes virulence through its antioxidant activity. J Exp Med 202: 209-215.